Research Article | Vol. 26, No. 8 | 16 Apr 2018 | OPTICS EXPRESS 11055
Optics EXPRESS

Paraxial propagation of a class of Bessel-correlated fields

ATRI HALDER,* MATIAS KOIVUROVA, HENRI PARTANEN, AND JARI TURUNEN

Institute of Photonics, University of Eastern Finland, P. O. Box 111, FI-80101 Joensuu, Finland
**atri.halder@uef.fi*

Abstract: The propagation of a novel class of paraxial spatially partially coherent beams exhibiting Bessel-type correlations is studied in free space and in paraxial optical systems. We show that, under certain conditions, such beams can have functionally identical forms of the absolute value of the complex degree of spatial coherence not only at the source plane and in the far zone, but also at all finite propagation distances. Under these conditions the degree of spatial coherence properties of the field is a shape-invariant quantity, but the spatial intensity distribution is only approximately shape-invariant. The main properties of this class of model beams are demonstrated experimentally by passing a coherent Gaussian beam through a rotating wedge and measuring the coherence of the ensuing beams with a Young-type interferometer realized with a digital micromirror device.

OCIS codes: (030.1640) Coherence; (320.6629) Wave propagation.

References and links

1. L. Mandel and E. Wolf, *Coherence and Quantum Optics* (Cambridge University, 1995).
2. G. Gbur and T. Visser, "The structure of partially coherent fields," Progr. Opt. **55,** 285-341 (2010).
3. Y. Cai, Y. Chen, and F. Wang, "Generation and propagation of partially coherent beams with nonconventional correlation functions: a review," J. Opt. Soc. Am. A **31,** 2083–2096 (2014).
4. Y. Cai, Y. Chen, J. Yu, X. Liu, and L. Liu, "Generation of partially coherent beams," Progr. Opt. **62,** 157–223 (2017).
5. F. Gori, G. Guattari, and C. Padovani, "Modal expansion for J_0-correlated Schell-model sources," Opt. Commun. **64,** 311–316 (1987).
6. F. Gori, M. Santarsiero, and R. Borghi, "Modal expansion for J_0-correlated electromagnetic sources," Opt. Lett. **33,** 1857–1859 (2008).
7. C. Palma and G. Cincotti, "Imaging of J_0-correlated Bessel-Gauss beams," IEEE J. Quantum Electron. **33,** 1032–1040 (1997).
8. R. Borghi, "Superposition scheme for J_0-correlated partially coherent sources," IEEE J. Quantum Electron. **35,** 849–856 (1999).
9. F. Gori, M. Santarsiero, R. Borghi, and C. F. Li, "Partially correlated thin annular sources: The scalar case," J. Opt. Soc. Am. A **25,** 2826–2832 (2008).
10. M. Santarsiero, V. Ramírez-Sánchez, and R. Borghi, "Partially correlated thin annular sources: The vectorial case," J. Opt. Soc. Am. A **27,** 1450–1456 (2010).
11. J. Turunen and A. T. Friberg, "Propagation-invariant optical fields," Progr. Opt. **54,** 1–88 (2009).
12. J. M. Durnin, J. J. Miceli, and J. H. Eberly, "Diffraction-free beams," Phys. Rev. Lett. **58,** 1499–1501 (1987).
13. F. Gori, "Collett-Wolf sources and multimode lasers," Opt. Commun. **34,** 301–305 (1980).
14. A. Starikov and E. Wolf, "Coherent-mode representation of Gaussian Schell-model sources and their radiation fields," J. Opt. Soc. Am. **72,** 923–928 (1982).
15. F. Gori and C. Palma, "Partially coherent sources which give rise to highly directional light beams," Opt. Commun. **27,** 185–188 (1978).
16. F. Gori, "Directionality and spatial coherence," Opt. Acta **27,** 1025–1034 (1980).
17. F. Gori, "Mode propagation of the fields generated by Collett–Wolf Schell-model sources," Opt. Commun. **46,** 149–154 (1983).
18. P. Vahimaa and J. Turunen, "Finite-elementary-source model for partially coherent radiation," Opt. Express **14,** 1376–1381 (2006).
19. F. Gori and G. Guattari, "A new type of optical fields," Opt. Commun. **48,** 7–12 (1983).
20. R. Simon and N. Mukunda, "Twisted Gaussian Schell-model beams," J. Opt. Soc. Am. A **10,** 95–109 (1993).
21. A. T. Friberg, E. Tervonen, and J. Turunen, "Interpretation and experimental demonstration of twisted Gaussian Schell-model beams," J. Opt. Soc. Am. A **11,** 1818–1826 (1994).

#325052 https://doi.org/10.1364/OE.26.011055
Journal © 2018 Received 28 Feb 2018; revised 24 Mar 2018; accepted 24 Mar 2018; published 13 Apr 2018

Optics EXPRESS

22. M. Koivurova, A. Halder, H. Partanen, and J. Turunen, "Bessel-correlated supercontinuum fields," Opt. Express **25,** 23974–23988 (2017).
23. G. Cincotti, F. Gori and M. Santarsiero, "Generalized self-Fourier functions," J. Phys. A: Math. Gen. **25(20),** L1191-L1194 (1992).
24. S. A. Collins, "Lens-system diffraction integral written in terms of matrix optiics," J. Opt. Soc. Am. **60,** 1168–1177 (1970).
25. A. T. Friberg and J. Turunen, "Imaging of Gaussian Schell-model sources," J. Opt. Soc. Am. A **5,** 713–720 (1988).
26. H. Partanen, J. Turunen, and J. Tervo, "Coherence measurement with digital micromirror device," Opt. Lett. **39,** 1034–1037 (2014).

1. Introduction

Partially spatially coherent model sources and light beams generated by them have attracted a great deal of interest over the past few decades. Apart from classical Gaussian Schell-model (GSM) sources and beams [1], a large number of fields with more unconventional correlation properties have been introduced and demonstrated, which exhibit a wide variety of interesting propagation properties and applications [2–4]. Among these, Bessel-correlated fields originally introduced by Gori [5] are particularly interesting [6–10]. This type of fields can be generated, e.g., by collimating light emitted by a spatially incoherent ring source. They can be (approximately) propagation-invariant in the sense that the spatial coherence coherence properties remain nearly unchanged as the field traverses forward over considerable distances [11]. As such, they can be viewed as generalizations of fully coherent Bessel fields [12] into the domain of partially coherent optics.

While no fields with a finite spatial extent can possess the property of strict propagation-invariance, a less strict condition of shape-invariant propagation can sometimes be satisfied. By this we refer to fields that experience only a scale change of the intensity distribution upon propagation. An even less strict condition is that the field at the source plane is of the same functional form as the radiation field in the far zone; we will call fields that behave in this matter as being self-Fourier-transforming. Hermite–Gaussian and Laguerre–Gaussian laser beams are well-known examples of fully coherent fields that are both shape-invariant and self-Fourier-transforming. Partially coherent fields that satisfy these criteria are also known. These include standard GSM fields, which can be thought of as superpositions of either laser modes [13–15] or 'elementary' spatially or angularly displaced Gaussian beams [16–18]. Such superpositions can also lead to spatially partially coherent fields with anisotropic shape-invariant intensity distributions extending from the source plane to the far zone, which is not possible with fully coherent fields [19]. Moreover, partially coherent beams with properties not shared by coherent beams, such as twist phase [20], can also be described using coherent-mode superpositions [21]. It is therefore safe to state that partial spatial coherence adds new degrees of freedom to optical beam formation, which motivates further studies on the subject.

We have recently introduced a class of Bessel-correlated fields, which can be generated by particularly simple experimental techniques: passing a coherent light beam through a rotating tilted glass plate or wedge [22]. Under certain conditions the cross-spectral density function at the source plane and the angular correlation function were found to have the same functional form. In this sense the fields introduced in [22, 23], behave like self-Fourier-transforming fields. In this paper we consider the paraxial propagation of this class of Bessel-correlated fields both analytically end experimentally.

The paper is structures as follows. In Sect. 2 we summarize briefly the main results of [22]. The propagation of these fields in free space and in first-order optical systems is discussed in Sects. 3–5, with particular attention to self-Fourier-transforming fields in Sect. 4. It is shown, e.g., that the absolute value of the complex degree of spatial coherence of these beams is a shape-invariant quantity if the condition for self-Fourier-transformation is satisfied. However, the beam intensity distribution is not strictly shape-invariant, and in this sense the behavior of the

Optics EXPRESS

model fields considered here is different from those radiated by GSM sources [17]. Experimental verifications of the main results are provided in Sect. 6, and conclusions are drawn in Sect. 7.

2. Source model

Figure 1 illustrates the geometry to be considered in our experiments, and it represents a simple method to generate model fields discussed below. Here a coherent Gaussian beam with its waist at the plane $z = 0$ is incident on a rotating prism with axial thickness d, wedge angle α, and refractive index n. When the wedge rotates about the z axis, the axial ray draws a circle of radius $R = d \tan(\alpha - \alpha')$, with $\alpha' = \arcsin(\sin\alpha/n)$, on the rear face of the wedge (at $z = 0$) and propagates at an angle $\beta = \arcsin[n \sin(\alpha - \alpha')]$ with respect to the z axis. At each instant of time a Gaussian beam propagating in the direction of this ray emerges; upon rotation of the wedge a partially spatially coherent field consisting of all such 'elementary' fields is generated in time-averaged sense. We describe it with a cross-spectral density function, considering the CSD in the sense of ensemble averaging with the elementary fields acting as realizations with equal probability of occurrence.

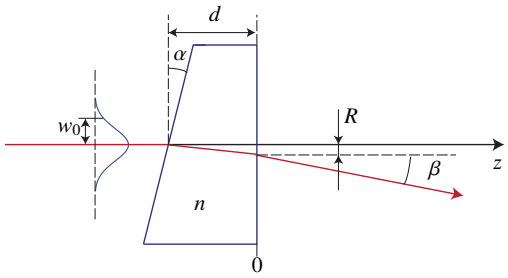

Fig. 1. Geometry. A Gaussian beam with $1/e^2$ waist radius w_0 is incident on a rotating prism with wedge angle α, central thickness d, and refractive index n. In the paraxial domain (small values of α) the output beam at $z = 0$ is a spatially displaced [by $R \approx d\alpha(1 - 1/n)$] and angularly deflected [by $\beta \approx \alpha(n - 1)$] Gaussian beam.

The cross-spectral density function (CSD) of the field that emerges from the wedge in the geometry of Fig. 1 can be described (at any plane $z \geq 0$) by an elementary-field superposition [22]

$$W(x_1, y_1, x_2, y_2, z) = \frac{1}{2\pi} \int_0^{2\pi} e^*(x_1, y_1, z; \phi) e(x_2, y_2, z; \phi) \mathrm{d}\phi, \tag{1}$$

where a single elementary-field contribution $e(x, y, z; \phi)$ depends on the (time-varying) azimuth angle ϕ. When the wedge is illuminated by a coherent Gaussian beam, the emerging Gaussian elementary field at the exit plane $z = 0$ of the wedge can be expressed as

$$e(x, y, 0; \phi) = e_0 \exp\left[-\frac{(x - R\cos\phi)^2 + (y - R\sin\phi)^2}{w_0^2}\right] \exp\left[ik_0 \sin\beta\,(x\cos\phi + y\sin\phi - R)\right], \tag{2}$$

where $k_0 = 2\pi/\lambda_0$ is the vacuum wave number. At the plane $z = 0$ the CSD then becomes

$$W(x_1, y_1, x_2, y_2, 0) = S_0 \exp\left(-\frac{x_1^2 + x_2^2 + y_1^2 + y_2^2 + 2R^2}{w_0^2}\right) I_0\left[a(x_1, y_1, x_2, y_2, 0)\right], \tag{3}$$

Optics EXPRESS

where $S_0 = |e_0|^2$, I_0 is the zeroth-order modified Bessel function,

$$a(x_1, y_1, x_2, y_2, 0) = \frac{4R}{w_0^2}\left[\left(\bar{x} - i\frac{z_R \sin\beta}{R}\frac{\Delta x}{2}\right)^2 + \left(\bar{y} - i\frac{z_R \sin\beta}{R}\frac{\Delta y}{2}\right)^2\right]^{1/2}, \tag{4}$$

and $z_R = k_0 w_0^2/2$ is the Rayleigh range of the incident Gaussian beam. In writing Eq. (4) we have introduced average spatial coordinates $\bar{x} = \frac{1}{2}(x_1 + x_2)$, $\bar{y} = \frac{1}{2}(y_1 + y_2)$ as well as difference spatial coordinates $\Delta x = x_2 - x_1$, $\Delta y = y_2 - y_1$. The intensity distribution at $z = 0$ is given by

$$S(x, y, 0) = W(x, x, y, y, 0) = S_0 \exp\left[-\frac{2\left(x^2 + y^2 + R^2\right)}{w_0^2}\right] I_0\left[\frac{4R}{w_0^2}\sqrt{x^2 + y^2}\right] \tag{5}$$

and the complex degree of spatial coherence takes the form

$$\begin{aligned}\mu(x_1, x_2, y_1, y_2, 0) &= \frac{W(x_1, x_2, y_1, y_2, 0)}{\sqrt{S(x_1, y_1, 0)S(x_2, y_2, 0)}} \\ &= \frac{I_0\left[a(x_1, y_1, x_2, y_2, 0)\right]}{\sqrt{I_0\left[a(x_1, y_1, x_1, y_1, 0)\right] I_0\left[a(x_2, y_2, x_2, y_2, 0)\right]}}.\end{aligned} \tag{6}$$

This is the class of Bessel-correlated model sources introduced in [22], where also the limiting cases $R \to 0$ and $\beta \to 0$ were considered in detail.

3. Propagation in free space

By inserting from Eq. (2) into the standard Fresnel formula

$$\begin{aligned}e(x, y, z; \phi) = &\frac{k_0}{i2\pi z}\exp(ik_0 z)\exp\left[\frac{ik_0}{2z}\left(x^2 + y^2\right)\right] \\ &\times \iint_{-\infty}^{\infty} e(x', y', 0; \phi)\exp\left[\frac{ik_0}{2z}\left(x'^2 + y'^2\right)\right]\exp\left[-\frac{ik_0}{z}\left(xx' + yy'\right)\right]\mathrm{d}x'\mathrm{d}y'\end{aligned} \tag{7}$$

for free-space propagation and carrying out the integrations, we obtain an expression for the elementary field at any propagation distance in the form

$$\begin{aligned}e(x, y, z; \phi) = &\frac{e_0}{1 + iz/z_R}\exp\left[ik_0 z\left(1 - \frac{1}{2}\frac{\sin^2\beta}{1 + iz/z_R}\right)\right]\exp\left[-\frac{(x - R\cos\phi)^2 + (y - R\sin\phi)^2}{w_0^2(1 + iz/z_R)}\right] \\ &\times \exp\left[\frac{ik_0 \sin\beta}{1 + iz/z_R}(x\cos\phi + y\sin\phi - R)\right].\end{aligned} \tag{8}$$

On inserting this expression into Eq. (1) we arrive at

$$\begin{aligned}W(x_1, y_1, x_2, y_2, z) = &\frac{|e_0|^2}{1 + (z/z_R)^2} \\ &\times \exp\left[-k_0 z_R \sin^2\beta\frac{(z/z_R)^2}{1 + (z/z_R)^2}\right]\exp\left[-\frac{x_1^2 + y_1^2 + R^2}{w_0^2(1 - iz/z_R)}\right]\exp\left[-\frac{x_2^2 + y_2^2 + R^2}{w_0^2(1 + iz/z_R)}\right] \\ &\times \frac{1}{2\pi}\int_0^{2\pi}\exp\left\{\left[c(z)\bar{x} - id(z)\Delta x/2\right]\cos\phi + \left[c(z)\bar{y} - id(z)\Delta y/2\right]\sin\phi\right\}\mathrm{d}\phi,\end{aligned} \tag{9}$$

where

$$c(z) = \frac{4}{w_0^2}\frac{R + z\sin\beta}{1 + (z/z_R)^2} = \frac{4R}{w^2(z)}\left(1 + \frac{z}{R}\sin\beta\right), \tag{10}$$

Optics EXPRESS

$$d(z) = 2k_0 \frac{Rz/z_R^2 + \sin\beta}{1 + (z/z_R)^2} = \frac{4R}{w^2(z)} \left(\frac{z}{z_R} + \frac{z_R}{R} \sin\beta \right), \tag{11}$$

and

$$w(z) = w_0 \left[1 + (z/z_R)^2 \right]^{1/2}. \tag{12}$$

The integration in Eq. (9) then gives

$$W(x_1, y_1, x_2, y_2, z) = S_0 \frac{w_0^2}{w^2(z)} \exp\left[-\frac{x_1^2 + x_2^2 + y_1^2 + y_2^2 + 2(R - z\sin\beta)^2}{w^2(z)} \right] \times I_0 \left[a(x_1, y_1, x_2, y_2, z) \right] \exp\left[\frac{ik_0}{2R(z)} \left(x_2^2 - x_1^2 + y_2^2 - y_1^2 \right) \right], \tag{13}$$

where

$$\begin{aligned} a(x_1, y_1, x_2, y_2, z) &= \left\{ [c(z)\bar{x} - id(z)\Delta x/2]^2 + [c(z)\bar{y} - id(z)\Delta y/2]^2 \right\}^{1/2} \\ &= \frac{4R}{w^2(z)} \left\{ \left[\left(1 + \frac{z}{R}\sin\beta \right) \bar{x} - i \left(\frac{z}{z_R} + \frac{z_R}{R}\sin\beta \right) \frac{\Delta x}{2} \right]^2 \right. \\ &\quad \left. + \left[\left(1 + \frac{z}{R}\sin\beta \right) \bar{y} - i \left(\frac{z}{z_R} + \frac{z_R}{R}\sin\beta \right) \frac{\Delta y}{2} \right]^2 \right\}^{1/2} \end{aligned} \tag{14}$$

and

$$R(z) = z + z_R^2/z. \tag{15}$$

The intensity distribution $S(x, y, z) = W(x, y, x, y, z)$ of the field reads as

$$S(x, y, z) = S_0 \frac{w_0^2}{w^2(z)} \exp\left\{ -\frac{2}{w^2(z)} \left[x^2 + y^2 + (R - z\sin\beta)^2 \right] \right\} I_0 \left[\frac{4R}{w^2(z)} \left(1 + \frac{z}{R}\sin\beta \right) \sqrt{x^2 + y^2} \right]. \tag{16}$$

and the complex degree of coherence has the form

$$\mu(x_1, x_2, y_1, y_2, z) = \frac{I_0 \left[a(x_1, y_1, x_2, y_2, z) \right]}{\sqrt{I_0 \left[a(x_1, y_1, x_1, y_1, z) \right] I_0 \left[a(x_2, y_2, x_2, y_2, z) \right]}} \exp\left[\frac{ik_0}{2R(z)} \left(x_2^2 - x_1^2 + y_2^2 - y_1^2 \right) \right]. \tag{17}$$

Clearly, $w(z)$ and $R(z)$ are the standard propagation parameters (beam width and radius of wavefront curvature) of the incident Gaussian beam at propagation distance z, which are determined by the initial beam width w_0. In addition, the parameters R and β related to the rotating wedge appear in the expressions of the CSD and the transverse intensity profile.

In the far zone $z \gg z_R$ we may approximate, as usual in the theory of Gaussian beams, $w(z) \to w_0 z/z_R = 2z/k_0 w_0$ and $R(z) \to z$. Then the CSD takes the asymptotic form

$$W^{(\infty)}(x_1, y_1, x_2, y_2, z) = S_0 \left(\frac{z_R}{z} \right)^2 \exp\left[-\left(\frac{z_R}{z} \right)^2 \frac{x_1^2 + x_2^2 + y_1^2 + y_2^2 + 2(R - z\sin\beta)^2}{w_0^2} \right] \times I_0 \left[a^{(\infty)}(x_1, y_1, x_2, y_2, z) \right] \exp\left[\frac{ik_0}{2z} \left(x_2^2 - x_1^2 + y_2^2 - y_1^2 \right) \right] \tag{18}$$

Optics EXPRESS

with

$$a^{(\infty)}(x_1, y_1, x_2, y_2, z) = \frac{2Rk_0}{z}\left[\left(\frac{z_R}{R}\sin\beta\bar{x} - i\frac{\Delta x}{2}\right)^2 + \left(\frac{z_R}{R}\sin\beta\bar{y} - i\frac{\Delta y}{2}\right)^2\right]^{1/2}. \quad (19)$$

The intensity distribution in the far zone is

$$S^{(\infty)}(x, y, z) = S_0\left(\frac{z_R}{z}\right)^2 \exp\left[-2\left(\frac{z_R}{z}\right)^2 \frac{x^2 + y^2 + z^2\sin^2\beta}{w_0^2}\right] I_0\left[2k_0\sin\beta\frac{z_R}{z}\sqrt{x^2 + y^2}\right] \quad (20)$$

and the far-zone complex degree of coherence has the form

$$\mu^{(\infty)}(x_1, y_1, x_2, y_2, z) = \frac{I_0\left[a^{(\infty)}(x_1, y_1, x_2, y_2, z)\right]}{\sqrt{I_0\left[a^{(\infty)}(x_1, y_1, x_1, y_1, z)\right] I_0\left[a^{(\infty)}(x_2, y_2, x_2, y_2, z)\right]}} \exp\left[\frac{ik_0}{2z}\left(x_2^2 - x_1^2 + y_2^2 - y_1^2\right)\right]. \quad (21)$$

These results are obtained also by inserting Eqs. (20) and (21) of [22], into the paraxial forms of the far-field formulas for the CSD presented, e.g., in Sect. 5.3 of [1].

4. Propagation of self-Fourier-transforming fields

Expressions (13)–(19) are valid for any combination of the parameters R and β. However, as demonstrated in [22], a particularly interesting class of fields is obtained if the condition

$$z_R\sin\beta = R \quad (22)$$

holds. This condition means that the backward-continuation of the local optical axis of the elementary Gaussian beam crosses the z axes at a distance $z = -z_R \approx -d/n$, implying that $w_0 \approx \sqrt{d\lambda_0/\pi n}$.

If condition (22) is satisfied, the field is self-Fourier-transforming, i.e., the functional forms of the CSD at the plane $z = 0$ and the angular correlation function are precisely the same [22]. At $z = 0$ we have, from Eq. (4),

$$a(x_1, y_1, x_2, y_2, 0) = \frac{4R}{w_0^2}\left[(\bar{x} - i\Delta x/2)^2 + (\bar{y} - i\Delta y/2)^2\right]^{1/2}. \quad (23)$$

In the far zone Eq. (19) reduces to

$$a^{(\infty)}(x_1, y_1, x_2, y_2, z) = \frac{2Rk_0}{z}\left[(\bar{x} - i\Delta x/2)^2 + (\bar{y} - i\Delta y/2)^2\right]^{1/2}. \quad (24)$$

Let us next introduce normalized transverse coordinates $x(z) = xz_R/z$, $y(z) = yz_R/z$, and similarly for $\bar{x}(z)$, $\bar{y}(z)$, $\Delta x(z)$, and $\Delta y(z)$. With these conventions we can write Eq. (19) as

$$a^{(\infty)}(x_1, y_1, x_2, y_2, z) = \frac{4R}{w_0^2}\left\{[\bar{x}(z) - i\Delta x(x)/2]^2 + [\bar{y}(z) - i\Delta y(z)/2]^2\right\}^{1/2}. \quad (25)$$

This result is identical in functional form with Eq. (4). Therefore the absolute value of the complex degree of spatial coherence in the far zone has the same shape as it has in the plane $z = 0$. In the scaled coordinates Eq. (20) reduces to

$$S^{(\infty)}(x, y, z) = S_0\left(\frac{z_R}{z}\right)^2 \exp\left\{-\frac{2\left[x^2(z) + y^2(z) + R^2\right]}{w_0^2}\right\} I_0\left[\frac{4R}{w_0^2}\sqrt{x^2(z) + y^2(z)}\right]. \quad (26)$$

Optics EXPRESS

Hence also the intensity distributions $S(x, y, 0)$ and $S^{(\infty)}(x, y, z)$ are of the same form.

Let us next examine the implications of condition (22) at an arbitrary propagation distance. If this condition holds, Eq. (14) reduces to

$$a(x_1, y_1, x_2, y_2, z) = \frac{4R}{w^2(z)}\left(1 + \frac{z}{z_R}\right)\left[(\bar{x} - i\Delta x/2)^2 + (\bar{y} - i\Delta y/2)^2\right]^{1/2}. \tag{27}$$

It follows from Eq. (16) that the transverse intensity profile of the field takes the form

$$S(x, y, z) = S_0 \exp\left\{-\frac{2}{w^2(z)}\left[x^2 + y^2 + R^2\left(1 - \frac{z}{z_R}\right)^2\right]\right\} I_0\left[\frac{4R}{w^2(z)}\left(1 + \frac{z}{z_R}\right)\sqrt{x^2 + y^2}\right]. \tag{28}$$

The complex degree of spatial coherence has the same form as in Eq. (17), with $a(x_1, y_1, x_2, y_2, z)$ given by Eq. (27). Hence its absolute value depend on the function $a(x_1, y_1, x_2, y_2, z)$ alone. Let us next generalize the definition of the scaled transverse coordinates into the form

$$x(z) = x\frac{1 + z/z_R}{1 + (z/z_R)^2}, \quad y(z) = y\frac{1 + z/z_R}{1 + (z/z_R)^2}, \tag{29}$$

and analogously for $\bar{x}(z)$, $\bar{y}(z)$, $\Delta x(z)$, and $\Delta y(z)$. We note that, in the far zone, these definitions reduce to the previously defined scaled coordinates, and at $z = 0$ to the actual spatial coordinates at that plane. We then find that

$$a(x_1, y_1, x_2, y_2, z) = \frac{4R}{w_0^2}\left\{[\bar{x}(z) - i\Delta x(z)/2]^2 + [\bar{y}(z) - i\Delta y(z)/2]^2\right\}^{1/2} \tag{30}$$

and therefore $|\mu(x_1, y_1, x_2, y_2, z)|$ is a shape-invariant quantity at all propagation distances. The only propagation-induced change in $\mu(x_1, y_1, x_2, y_2, z)$ is the quadratic phase factor.

The condition for shape-invariant propagation does not extend to the transverse intensity distribution. Using the modified scaled coordinates introduce in Eq. (29) we can cast Eq. (28) in the form

$$S(x, y, z) = S_0\frac{w_0^2}{w^2(z)}\exp\left(-\frac{2}{w_0^2}\frac{1 + (z/z_R)^2}{(1 + z/z_R)^2}\left\{x^2(z) + y^2(z) + R^2\left[\frac{1 - (z/z_R)^2}{1 + (z/z_R)^2}\right]^2\right\}\right)$$
$$\times I_0\left[\frac{4R}{w_0^2}\sqrt{x^2(z) + y^2(z)}\right], \tag{31}$$

which implies that the Bessel contribution to the intensity profile is shape-invariant but the Gaussian contribution is not. Figure 2 illustrates the scaling of the transverse spatial coordinates given by Eq. (29) in comparison with the scaling

$$x(z) = x\left[1 + (z/z_R)^2\right]^{-1}, y(z) = y\left[1 + (z/z_R)^2\right]^{-1} \tag{32}$$

of the coordinates of the incident Gaussian beam required to transform it (mathematically) into a propagation-invariant form. While the latter is a monotonously decreasing function of z, the former initially increases, reaching a peak at $z/z_R = \sqrt{2} - 1$, where $x(z) = x\left(1/2 + 1/\sqrt{2}\right) \approx 1.21$.

Optics EXPRESS

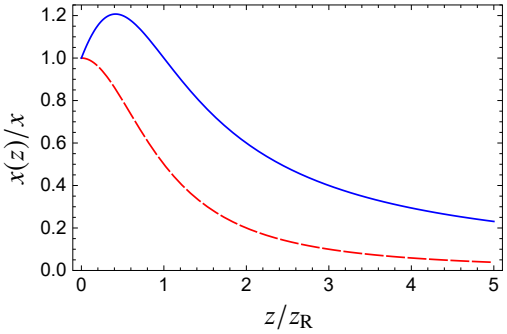

Fig. 2. Evolution of scaled coordinates for the complex degree of coherence of self-Fourier-transforming Bessel-correlated fields (blue solid line) and the incident Gaussian beam (red dashed line).

Propagation-invariant distributions of the absolute value of the complex degree of spatial coherence $|\mu(x_1, 0, x_2, 0, z)|$ are illustrated in Fig. 3. These distributions show strong variations of the antidiagonal width as a function of the average (diagonal) coordinate $\bar{x}(z)$, indicating that the fields are not of the Schell-model form (the coherence width depends on $\bar{x}$). A 'waist' of the coherence width is seen at $\bar{x}(z) = 0$, and the width of this waist narrows down as the normalized ratio $r = R/w_0$ increases.

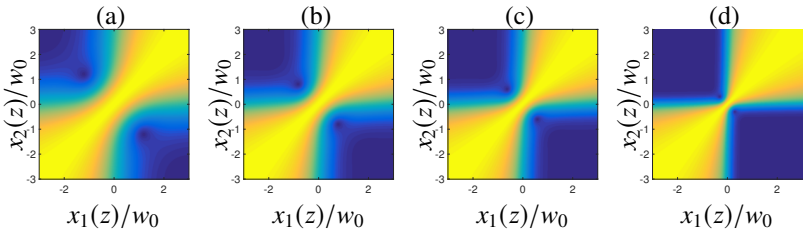

Fig. 3. Absolute values of the complex degree of spatial coherence of self-Fourier-transforming Bessel-correlated fields for various values of the ratio $r = R/w_0$. (a) $r = 0.5$. (b) $r = 0.75$. (c) $r = 1$. (d) $r = 2$.

Figure 4 shows intensity distributions self-Fourier-transforming fields in scaled coordinates. The dependence of the intensity profile at $z = 0$ on $r = R/w_0$ is illustrated in Fig. 4(a). When r exceeds ~ 0.75, a dip appears in the center of the intensity profile. This dip deepens with increasing r, and the beam takes on a doughnut shape as the Bessel contribution becomes dominant. The propagation of a beam with $r = 0.5$ is illustrated in Fig. 4(b). Since the Gaussian contribution still affects the intensity profile significantly, the shape varies with propagation distance. However, when $r > 0.75$, these changes become nearly indistinguishable (at least within the plotting accuracy of figures) and hence also the spatial profile becomes virtually shape-invariant.

Optics EXPRESS

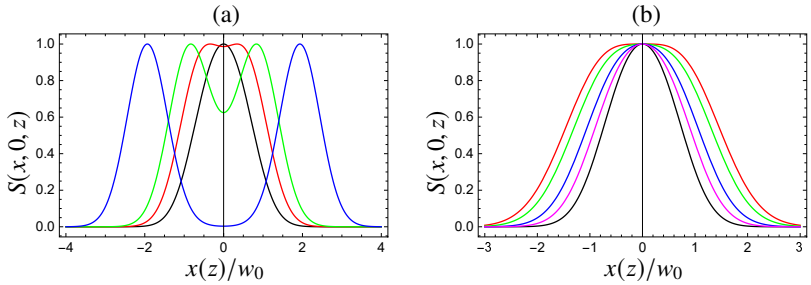

Fig. 4. Intensity profiles of self-Fourier-transforming Bessel-correlated fields. (a) Profiles at $z = 0$ for various values of $r = R/w_0$. Black: $r = 0.5$. Red: $r = 0.75$. Green: $r = 1$. Blue: $r = 2$. (b) Profiles with $r = 0.5$ at distances $z = 0$ (black), $z = z_R$ (red), $z = 2z_R$ (green), $z = 4z_R$ (blue), and $z = 8z_R$ (purple). For clarity the profiles have been normalized to their maximum values.

5. Propagation in paraxial systems

Wave propagation of the elementary field in a rotationally symmetric paraxial systems characterized by a 2×2 ABCD matrix is governed by the generalized Fresnel formula [24]

$$e(x, y, L; \phi) = \frac{k_0}{i2\pi B} \exp(ik_0 L) \exp\left[\frac{ik_0 D}{2B}\left(x^2 + y^2\right)\right] \times \iint_{-\infty}^{\infty} e(x', y', 0; \phi) \exp\left[\frac{ik_0 A}{2B}\left(x'^2 + y'^2\right)\right] \exp\left[-\frac{ik_0}{B}\left(xx' + yy'\right)\right] \mathrm{d}x'\mathrm{d}y', \tag{33}$$

where L is the axial path length through the system. By inserting from Eq. (2), performing the integrations, and simplifying we obtain

$$e(x, y, L; \phi) = \frac{e_0}{A + iB/z_R} \exp(ik_0 L) \exp\left(-\frac{ik_0}{2}\frac{B\sin^2\beta}{A + iB/z_R}\right) \exp\left(-\frac{R^2}{w_0^2}\frac{A}{A + iB/z_R}\right) \times \exp\left(-ik_0 R \sin\beta \frac{A}{A + iB/z_R}\right) \exp\left[\frac{ik_0}{2}\frac{C + iD/z_R}{A + iB/z_R}\left(x^2 + y^2\right)\right] \times \exp\left[ik_0 \frac{\sin\beta - iR/z_R}{A + iB/z_R}\left(x\cos\phi + y\sin\phi\right)\right], \tag{34}$$

where the ABCD matrix determinant relation $AD - BC = 1$ was used.

It is useful, at this stage, to introduce the propagation parameters of Gaussian beams in rotationally symmetric ABCD systems:

$$w_L = w_0 \left[A^2 + (B/z_R)^2\right]^{1/2} \tag{35}$$

and

$$R_L = \frac{A^2 + (B/z_R)^2}{AC + BD/z_R^2}. \tag{36}$$

These expressions give the beam width and radius of curvature at the output plane of an ABCD system for axial Gaussian beams if a beam waist is located at the input plane of the system. They apply to Gaussian Schell-model beams as well, with an appropriate extension of the definition of

Optics EXPRESS

the Rayleigh range [25]. They are also extensions of the free-space propagation parameters $w(z)$ and $R(z)$ in Eqs. (12) and (15).

If we insert from Eq. (34) into Eq. (2) and make use of the propagation paramters just introduced, we can cast the CSD at the output plane of the ABCD system in the form

$$W(x_1, y_1, x_2, y_2, z) = S_0 \frac{w_0^2}{w_L^2} \exp\left[-\frac{x_1^2 + x_2^2 + y_1^2 + y_2^2 + 2\,(AR - B\sin\beta)^2}{w_L^2}\right] \times I_0\left[a(x_1, y_1, x_2, y_2, L)\right] \exp\left[\frac{ik_0}{2R_L}\left(x_1^2 - x_2^2 + y_1^2 - y_2^2\right)\right], \tag{37}$$

where

$$a(x_1, y_1, x_2, y_2, L) = \left[(c_L\bar{x} - id_L\Delta x/2)^2 + (c_L\bar{y} - id_L\Delta y/2)^2\right]^{1/2}, \tag{38}$$

$$c_L = \frac{4R}{w_L^2}\left(1 + \frac{B}{R}\sin\beta\right), \tag{39}$$

$$d_L = \frac{4R}{w_L^2}\left(\frac{B}{z_R} + \frac{Az_R}{R}\sin\beta\right). \tag{40}$$

These expressions reduce to the free-space propagation formulas derived in Sect. 3 in the special case $A = D = 1$, $B = L = z$, and $C = 0$.

6. Experimental verification

In this section we demonstrate two examples of Bessel-correlated fields: in the first example the condition (22) is approximately satisfied, while in the second example it is clearly violated. In both cases we measure both the degree of spatial coherence and the intensity profile across several planes and compare the results with theoretical simulations.

The experimental setup is presented schematically in Fig. 5. The light source is a single-mode HeNe laser operating at 633 nm. A beam forming system BE consisting of a zoom camera lens and an achromatic fixed focal length (8.57 mm) lens was aligned in such a way that it reduces the size of the beam waist according to our requirements. The system BF is closely afocal, and the demagnification could be varied from $\sim 2 - 10.5$ by changing the focal length of the zoom lens.

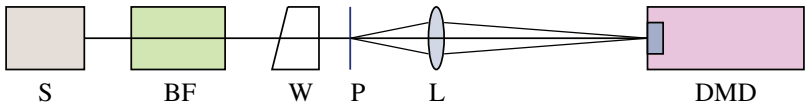

Fig. 5. Experimental setup: A is a single-mode HeNe laser source, BF a beam forming system, W the rotating wedge, L an imaging lens, DMD a digital micro-mirror device, and P is a plane at a (variable) distance z from the exit plane of the wedge.

A CCD sensor was used to find the axial position of the beam waist and to the measure its size w_0. The wedge W was then placed in the beam path so that the waist position formed by BE coincides with its exit plane. A positive lens L with 40 mm focal length was used to produce a magnified image of the plane P of interest to the DMD plane, with a magnification factor of ~ 5. The detailed working principle of the DMD can be found in [26]. The wedge was rotated around the optical axis with a reasonable angular speed compared to the integration time of the recording

Optics EXPRESS

device. Figure. 6 shows the simulated and measured two-point coherence functions, respectively, for the case when the condition (22) is nearly satisfied, and Fig. 7 shows cross-sectional beam intensity profiles at several distances.

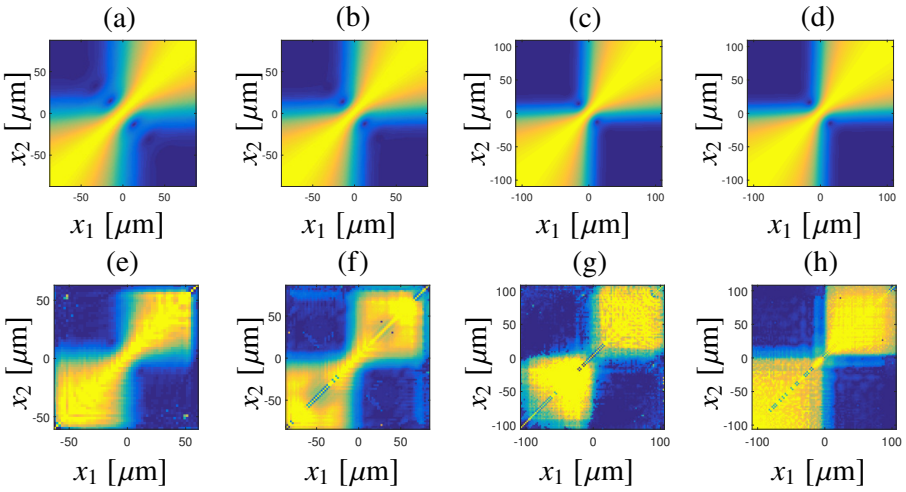

Fig. 6. Simulated (top row) and measured (bottom row) absolute value of the complex degree of spatial coherence in the (x_1, x_2) co-ordinate system when Eq. (22) is nearly satisfied: (a,e) $z = 0$ mm. (b,f) $z = 2$ mm. (c,g) $z = 4$ mm. (d,h) $z = 6$ mm. $w_0 \approx 40$ μm.

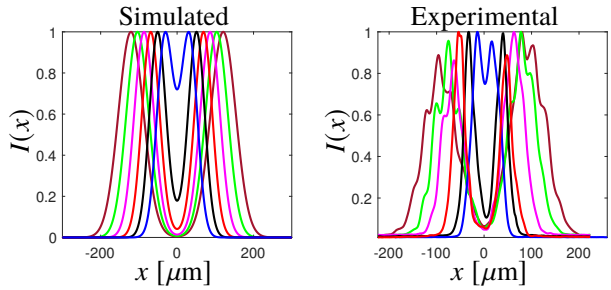

Fig. 7. Intensity cross-sections at $y = 0$ μm when (22) is nearly satisfied. Blue: $z = 0$ mm. Black: $z = 2$ mm. Red: $z = 4$ mm. Pink: $z = 6$ mm. Green: $z = 8$ mm. Maroon: $z = 10$ mm. $w_0 \approx 40$ μm.

We used a 6.5 mm thick glass wedge with a prism angle of 1°, which deviates the beam by $\sim 0.5°$ from its path. With these parameters the desired beam waist size, according to Eq. (22), is $w_0 \sim 29$ μm ($R \approx 39$ μm). However, in the experimental setup $w_0 \approx 40$ μm was the smallest attainable waist size. Hence condition (22) could not be satisfied exactly. However, in view of the simulations in Fig. 6, carried out with the actual experimental parameters, the absolute value of the complex degree of spatial coherence is nearly shape-invariant.

The two-point degree of spatial coherence was measured at four planes, including the source plane $z = 0$. With the chosen parameters $z_R \approx 4$ mm, and the measurements extended to a distance of $z = 1.5z_R = 6$ mm from the source plane. Intensity measurements were made up to a distance $z = 10$ mm. Another set of experiments is illustrated in Figs. 8 and 9. Here we used a wedge thickness of 3.5 mm (with the same prism angle as above) and chose $w_0 = 100$ μm, which gives $z_R = 49$ mm. With these parameters the condition (22) is violated strongly and, as

Optics EXPRESS

we move away from the source plane by a distance that is only a small fraction of the Rayleigh range, the spatial coherence and intensity profiles already change drastically in both simulations and experiments. That clearly confirms that close satisfaction of (22) is a necessary condition for obtaining an essentially shape-invariant spatial coherence function.

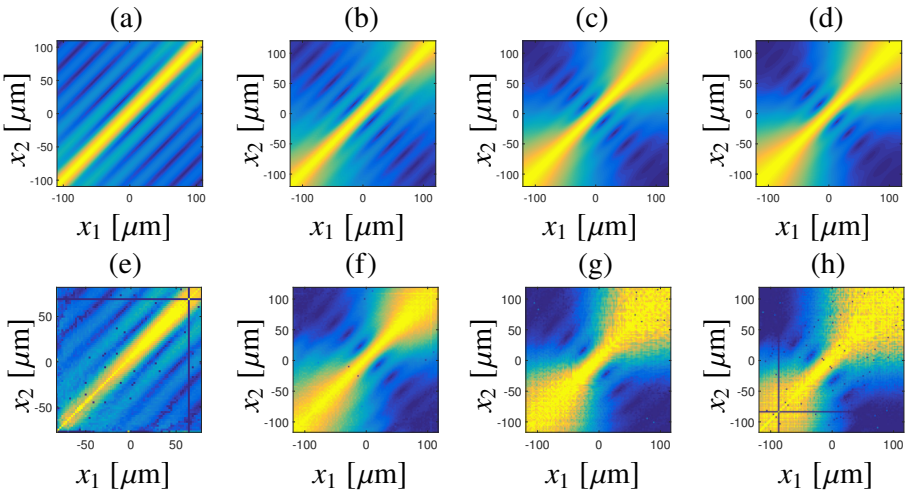

Fig. 8. Same as Fig. 6, but under experimental conditions where Eq. (22) is not satisfied: (a) $z = 0$ mm. (b) $z = 2$ mm. (c) $z = 4$ mm. (d) $z = 6$ mm. $w_0 \approx 100$ μm.

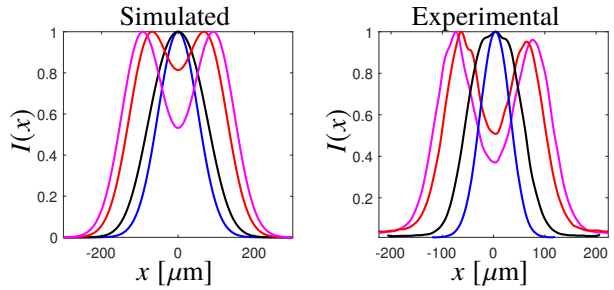

Fig. 9. Intensity cross-sections when (22) is not satisfied. Blue: $z = 0$ mm. Black: $z = 4$ mm. Red: $z = 8$ mm. Pink: $z = 10$ mm. $w_0 \approx 100$ μm.

The agreement between the simulated and experimental results is quite reasonable (though not perfect). In particular, several side lobes of the spatial coherence profile $|\gamma(x_1, x_2)|$ (in the antidiagonal direction) at short propagation distances are seen in Fig. 8 (also experimentally.) The departure of $|\gamma(x_1, x_2)|$ from the Schell-model form at larger propagation distances is likewise observed. The measurements were disturbed somewhat by interference effects due to back-reflections from the glass plate protecting the CCD sensor, which could not be completely eliminated. As we can see some asymmetry in case of Fig 9, was due to the rotational speed of the wedge glass plate was not very high, so while capturing the image for a particular plane of interest the intensity was not necessarily distributed uniformly through the whole ring shape. Additionally, reflections between the CCD surface and the protective glass created independent ring like interference pattern, which contributes to the asymmetry. This type of effects would be greatly reduced if a source with more limited temporal coherence were used for the experiments, such as a superluminescent diode. Small deviations between simulations and experiments also

Optics EXPRESS

undoubtedly arise from difficulties in measuring the beam width w_0 at a high precision, and placing the beam waist exactly at the exit plane of the wedge.

7. Conclusions

In conclusion, we have developed an analytical model for propagation of a novel class of spatially partially coherent, Bessel-correlated, fields in free space and paraxial optical systems. Here we considered only monochromatic fields, but the analysis can be extended to polychromatic stationary field and to pulsed fields. We have also considered only a generation scheme based on rotating wedges. Other types of rotating elements, in particular custom-designed diffractive elements, should provide considerable extra freedom in customizing the spatial coherence and may lead to a wider class of experimentally realizable fields with shape-invariant spatial coherence properties.

Funding

Academy of Finland (285880); Strategic funding of the University of Eastern Finland (930350).